

# Quantum wakes in lattice fermions

Matthew Wampler, Peter Schauss, Eugene B Kolomeisky, and Israel Klich  
*Department of Physics, University of Virginia, Charlottesville, VA, USA*

The wake following a vessel in water is a signature interference effect of moving bodies, and, as described by Lord Kelvin, is contained within a constant universal angle. However, wakes may accompany different kinds of moving disturbances in other situations and even in lattice systems. Here, we investigate the effect of moving disturbances on a Fermi lattice gas of ultracold atoms and analyze the novel types of wake patterns that may occur. We show how at half-filling, the wake angles are dominated by the ratio of the hopping energy to the velocity of the disturbance and on the angle of motion relative to the lattice direction. Moreover, we study the difference between wakes left behind a moving particle detector versus that of a moving potential or a moving particle extractor. We show that these scenarios exhibit dramatically different behavior at half-filling, with the "measurement wake" following an idealized detector vanishing, though the motion of the detector does still leave a trace through a "fluctuation wake." Finally, we discuss the experimental requirements to observe our predictions in ultracold fermionic atoms in optical lattices.

## INTRODUCTION

Many signature effects of classical hydrodynamics have counterparts in quantum systems and serve to provide intuition as well as a spectacular source for interesting new physical situations. Due to the absence of internal scale in hydrodynamics, it can be applied for physical scenarios of vastly different scales. For example, relativistic hydrodynamics has been successfully used to explain collective effects in heavy-ion collisions at RHIC and LHC [1]. On the other hand, studies of hydrodynamic-like effects in strongly interacting electron systems show unexpected effects due to their similarity to viscous fluids. For example, ref [2] shows that in certain situations, conductance may exceed Landauer's ballistic limit due to viscous effects, while ref. [3] demonstrates that slow "swimming" in a Fermi gas is of a topological nature, and can be fine-tuned to be done without dissipation.

Another interesting example of a hydrodynamics inspired study is the investigation of wake waves produced as a response to a moving potential interacting with a two-dimensional electron gas, recently described in [4]. There, it was pointed out that the pattern formed is determined by a Mach number and has similarities to Kelvin wakes in water and to Mach shock waves following a supersonic projectile. This behavior can be traced to the coherent interference between plasma excitations in the medium, with a dispersion which is water-like ( $\omega(q)^2 \propto q$ ) at long wavelengths. A related effect, Cerenkov radiation due to a moving charge in a dielectric has also been studied extensively, most recently in photonic crystals where a host of new variations on the effect have been uncovered where, for example, the direction of radiated energy can be flipped see e.g. [5, 6].

Here, we consider an altogether different system and, with it, a new set of non-equilibrium problems. We examine the discrete-time steady-state generated by the interaction of different types of disturbances, as described below, with fermions on a lattice, as the disturbances

move from site to site. Thus, the discrete time, the lattice and the many-body nature of the system play essential roles in the definition of our model. We find that some types of disturbances, not available in the above mostly classical scenarios may yield a drastically different response. The case in point is that of a moving quantum particle detector, which in this context has no classical counterpart. In addition, we study a moving particle extraction site, in which particles can be ejected out of the system. These two types of disturbances are compared with results we obtain for a moving potential. We note that moving detectors have been considered before, most notably in describing the Unruh effect [7], where a uniformly accelerated detector observes a thermal radiation in vacuum. However, the question we consider here seems to be completely new: what type of a steady state density pattern will a moving detector leave behind when measuring particle densities in a Fermi sea.

The recent progress of quantum simulation with ultracold atoms [8] makes them an ideal platform for studying these effects. Here, we focus on cold Fermi gases which became a valuable tool in recent years to study non-equilibrium dynamics in analogy to electronic systems. Indeed, recently, an increasingly sophisticated techniques became accessible leading to the measurement of spin dynamics [9–11] and charge transport [12–14]. In particular, it also became possible to observe spin charge separation in one-dimensional lattice systems [15] and to study spin- and charge transport in the two-dimensional Fermi-Hubbard model in the regime of low temperatures and strong correlations that challenge current theory calculations [16, 17]. These experiments demonstrate that ultracold fermionic atoms are an effective platform for quantum simulation of non-equilibrium phenomena even beyond the capabilities of exact calculations.

Classically, the universality of wakes following moving ships has been characterized by Kelvin's seminal result, that a (gravity) wake behind a moving ship in water is delimited within a constant angle  $39^\circ$ , irrespective of the

ship's velocity [18]. Recent results emphasize finite-size effects [19] through the dependence on the Froude number  $v/\sqrt{gL}$  of a moving pressure source traveling at velocity  $v$  of length  $L$ , where  $g$  is the gravitational acceleration constant [20]. Here, we study wakes created by point disturbances moving through a Fermi lattice gas including the quantum effects (Fig. 1). Even for a point source, our results depend on both the velocity and the angle with respect to the Bravais lattice directions, as well as on the type of disturbance. Concretely, we consider a tip traveling through a lattice of cold fermionic atoms, interacting with an atom on a lattice site, and then during a time  $\tau$  moving on to the next site.

We find several unexpected results. For example, we observe a dramatic difference between the wakes of a moving particle detector and a traveling potential disturbance. Another surprising result is that, at half-filling, the wake formed by a "particle" extractor is independent of temperature. To find an analytic form for the wake left behind a moving potential we use a co-moving steady-state equation and employ a somewhat unusual strategy of identifying lines where the (co-moving) disturbance is exactly zero, in contrast to most treatments of water wakes. Due to the scale inherent in the lattice structure, our wakes depend explicitly on the time  $\tau$  characterizing the effective speed of the moving tip, compared to the hopping energy  $t_{hop}$  of the lattice fermions.

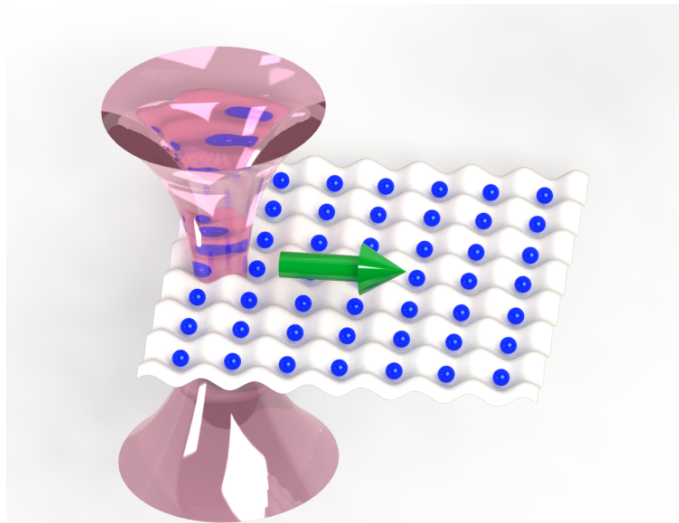


FIG. 1: A lattice of cold atoms interacting with a moving disturbance. The disturbance can be an applied potential, a detector or an extractor. The blue dots represent the fermionic atoms and the red focussed laser beam illustrates the disturbance moving into the direction of the green arrow.

To describe these effects of dynamics in many-particle quantum systems we use the non-equilibrium framework derived in [21]. This framework allows for the study of

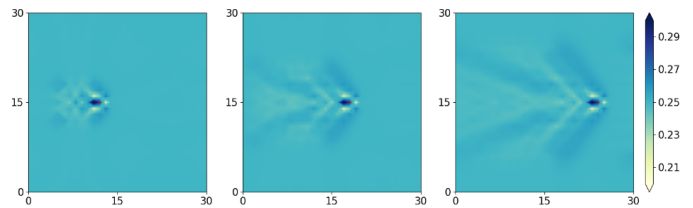


FIG. 2: A wake developing following a moving particle detector at quarter filling. The color bar on the right shows the particle density. The location of the disturbance is marked by a red dot.

a variety of non-equilibrium problems including particle detection and injection/extraction. It was shown in [21] that in certain statistical mechanics problems, it is possible to make a systematic connection between the evolution of  $n$  body density functions with  $n + 1$  density functions, similar in spirit to the Bogoliubov-Born-Green-Kirkwood-Yvon (BBGKY) hierarchy, which is the essential structure leading to the Boltzmann equation for single particle densities from higher order correlation functions (see, e.g. [22]). The range of possibilities using this approach is large, allowing the buildup of tractable non-equilibrium problems utilizing combinations of four elementary operations: detection, particle injection, particle extraction and free evolution. While some of these ideas have been applied to problems in 1D, here we study the emergence of wakes behind moving objects interacting with a Fermi sea. In particular, we discuss the difference between the motion of a detector and a potential in detail. The approach of [21] allows for an efficient numerical calculation of the dynamics in such problems. An example of the development of a wake a moving detector is described in Fig. 2, while a comparison between a moving detector and potential is provided in Fig. 3 at different filling fractions of a Fermi sea in a 2d hopping model.

The structure of the paper is as follows. We start by briefly introducing the formalism of [21]. Next we study the effect of a potential hopping from site to site, solving for the characteristic angles of the traveling pattern. We then continue to study the motion of a detector and the motion of a particle extractor and compare these with our results for the moving potential. Finally, we suggest an experimental setup to directly observe the wake patterns.

## FORMALISM

First, we provide a formal description of the system depicted in figure 1. We will denote by  $a_{\mathbf{r}}$  the annihilation operator for a fermion at lattice site  $\mathbf{r}$ . To describe the density and momentum distributions we will focus on the two point function, defined as:

$$G_{\mathbf{r}\mathbf{r}'} = \langle a_{\mathbf{r}}^{\dagger} a_{\mathbf{r}'} \rangle \quad (1)$$

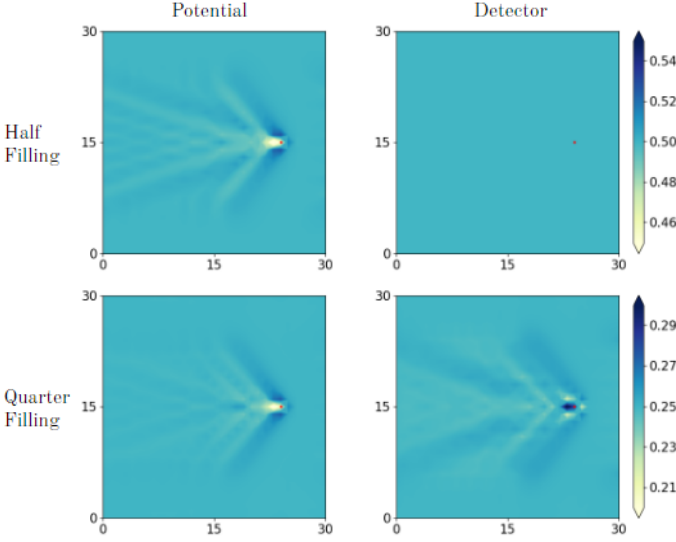


FIG. 3: Comparison of a wake developing following a moving point potential (left) with a moving detector (right). At half filling the difference is most dramatic (top) but differences remain at quarter filling (bottom).

The evolution of  $G_{\mathbf{r}\mathbf{r}'}$  depends on the problem at hand. Due to the discrete nature of the lattice, we find it convenient to consider the time evolution in discrete time steps  $\tau$ , pertaining to the time disturbance moves from site to site. After a step in the evolution process,  $G(t) \rightarrow \mathcal{K}(G) \equiv G(t + \tau)$ , where  $\mathcal{K}(G)$  is specified for various processes below.

For a non-interacting Hamiltonian,  $\mathcal{H}(t) = \sum_{\mathbf{r}\mathbf{r}'} H_{\mathbf{r}\mathbf{r}'}(t) a_{\mathbf{r}}^\dagger a_{\mathbf{r}'}$ , the evolution of  $G$  from time  $t$  to time  $t + \tau$  is given by:

$$G_{\mathbf{r}\mathbf{r}'}(t + \tau) = \text{Tr} \rho(t) \mathcal{U}^\dagger a_{\mathbf{r}}^\dagger a_{\mathbf{r}'} \mathcal{U} = [\mathcal{U} G(t) \mathcal{U}^\dagger]_{\mathbf{r}\mathbf{r}'} \equiv [\mathcal{K}_U(G)]_{\mathbf{r}\mathbf{r}'} . \quad (2)$$

where  $\mathcal{U} = \mathcal{T} e^{-\frac{i}{\hbar} \int_0^\tau \mathcal{H}(s) ds}$ , the associated single particle evolution is  $U = \mathcal{T} e^{-\frac{i}{\hbar} \int_0^\tau H(s) ds}$ , and the expectation value is computed using the density matrix at time  $t$ . Throughout the rest of the paper we will use units where  $\hbar = 1$ . Other operations require more elaborate transformations, as described in [21]. In particular, a particle detection measurement at a site  $\mathbf{r}$  induces the following map on  $G$ :

$$G \rightarrow \mathcal{K}_{\text{detect. } r}(G) = P_{\mathbf{r}}^\perp G P_{\mathbf{r}}^\perp + P_{\mathbf{r}} G P_{\mathbf{r}} . \quad (3)$$

where  $P_{\mathbf{r}}$  is the (single-particle) projector on site  $\mathbf{r}$ , while an extraction event of a particle at site  $\mathbf{r}$  can be described by the processes

$$G \rightarrow \mathcal{K}_{\text{extr. } r}(G) = P_{\mathbf{r}}^\perp G P_{\mathbf{r}}^\perp + (1 - \epsilon) P_{\mathbf{r}} G P_{\mathbf{r}}^\perp + (1 - \epsilon) P_{\mathbf{r}}^\perp G P_{\mathbf{r}} + (1 - \epsilon)^2 P_{\mathbf{r}} G P_{\mathbf{r}} . \quad (4)$$

where  $0 \leq \epsilon \leq 1$  describes the efficiency of the extraction procedure.

In our setup here, the disturbance will interact with the system at position  $\mathbf{r}$ , and moves to act on an adjacent point  $\mathbf{r} + a\mathbf{w}$ , where it acts again after which it moves to  $\mathbf{r} + 2a\mathbf{w}$  and so on.

For such a moving disturbance, a steady state can only be formed in the co-moving frame. In the discrete system, we define the steady state via the equation:

$$G = S^\dagger \mathcal{K}(G) S \quad (5)$$

where  $\mathcal{K}(G)$  is  $G$  after the operation and  $S$  is a translation operator along the direction of motion  $\mathbf{w}$ , i.e.  $S^\dagger \mathbf{r} = \mathbf{r} + a\mathbf{w}$ . In the following sections we consider different choices for  $\mathcal{K}(G)$ .

We use this formalism to investigate steady states using two main methods. First, we numerically simulate the moving disturbance by initializing the system in a non-interacting Fermi state, described by an initial two-point function  $G_0$ , and applying successively  $\mathcal{K}$  at site  $\mathbf{r}$ ,  $\mathbf{r} + a\mathbf{w}$ ,  $\mathbf{r} + 2a\mathbf{w}$ , and so on to generate the developed wake pattern, see e.g. Fig 2. Second, we solve explicitly for solutions to Eq. (5) to obtain analytic properties of the steady states of moving disturbances. It is important to note that for simplicity in this paper, we focus on non-interacting systems. However, the formalism is still valid for systems prepared in an interacting state as long as the subsequent unitary evolution is well approximated by non-interacting evolution.

## A MOVING POTENTIAL

Consider a tip traveling along the lattice, in a direction  $\mathbf{w}$ , exerting a potential  $V$  and taking a time  $\tau$  to move between two sites. We approximate this process as a discrete process, where the potential hops from site to site, remaining a time unit  $\tau$  at each site. For the purposes of this paper, we will focus on the simplest case of a square lattice with nearest neighbor hopping as the free evolution, i.e.  $\mathcal{H}_0 = -t_{\text{hop}} \sum_{\langle \mathbf{r}, \mathbf{r}' \rangle} a_{\mathbf{r}}^\dagger a_{\mathbf{r}'}$  with eigenvalues  $\varepsilon(k) = -2t_{\text{hop}} [\cos(k_x a) + \cos(k_y a)]$  where  $a$  is the lattice spacing. We will take the tip potential at a fixed reference point  $\mathbf{r}_0$  to be  $\mathcal{V} = V a_{\mathbf{r}_0}^\dagger a_{\mathbf{r}_0}$ . We will mostly concentrate on half filling in this section.

We describe below the wake formed behind a point potential moving at a general speed and angle with respect to the lattice. Fig. 4 shows the simulation of the wake pattern formed by evolving the system in real time following a successive application of the tip along a horizontal line moving at various speeds. Fig. 5 represents the simulation of the wake formed by similarly evolving the system in real time except with the tip moving at several different angles with respect to the lattice. Denoting

$$\alpha = \frac{1}{2\tau t_{\text{hop}}} \quad (6)$$

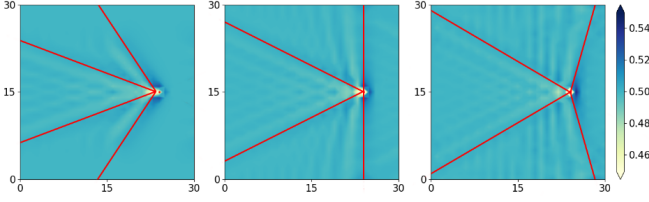


FIG. 4: Varying the velocity of a moving potential. From left to right, velocities  $\alpha = 1.7, 1.0$ , and  $0.7$ . Red lines represent the angles given by Eq. (29). Each line corresponds to the solution for a given quadrant in Fig. 6. Note the forward pointing cone is a result of a forward d-wave radiation when the source is moving slowly.

we use Eq. (5) to find that the angles of lines of zero disturbance are described by

$$\frac{r_y}{r_x} = \frac{1 + w_y \alpha}{\pm 1 + w_x \alpha} ; \quad \frac{r_y}{r_x} = \frac{-1 + w_y \alpha}{\pm 1 + w_x \alpha} \quad (7)$$

These "zero disturbance" lines are represented as red lines in the figures, and delineate the shape of the wake openings. As expected, since we are not in a Kelvin regime, the angle depends on the speed of the disturbance and is discussed below. Note, in contrast to the classic Kelvin wakes and potential wakes in a two-dimensional electron gas, here the lattice breaks rotational symmetry and the wake pattern changes as the potential path rotates with respect to the lattice.

Before moving on to the derivation, let us comment briefly on the limiting behavior of Eq. (7). Note, that as  $\alpha \rightarrow 0$ , we find  $\frac{r_y}{r_x} \rightarrow \pm 1$ , i.e. the two main diagonal directions. This result is consistent with the expectation that as the velocity vanishes, the moving potential is almost static and will radiate via the underlying D-wave symmetry of the lattice.

As  $\alpha \rightarrow \infty$ , i.e. the limit of an extremely fast moving tip, we find that  $\frac{r_y}{r_x} \rightarrow \frac{w_y}{w_x}$ , in other words, the wake converges onto a line following the disturbance, as any disturbance would not have time to disperse. Hence, Eq. (7) implies that the wake will essentially vanish for a potential moving at  $\alpha \rightarrow \infty$ .

The co-moving steady state to be found for our system is described by, Eq. (5), where  $\mathcal{K}(G) = e^{i\tau(H_0+V)} G e^{-i\tau(H_0+V)}$  where  $H_0$  described the unperturbed single particle system and  $V_{\mathbf{r}\mathbf{r}'} = V \delta_{\mathbf{r}\mathbf{r}'} \delta_{\mathbf{r}'\mathbf{r}_0}$  is the tip potential at some initial reference point  $\mathbf{r}_0$ . Namely:

$$S^\dagger e^{i\tau(H_0+V)} G e^{-i\tau(H_0+V)} S = G \quad (8)$$

In general, equation (8) admits infinitely many solutions for  $G$ . In particular, any correlation matrix  $G$  that satisfies:

$$[G, S^\dagger e^{i\tau(H_0+V)}] = 0 \quad (9)$$

will automatically be a co-moving non-equilibrium steady state. In the physical scenario we are interested in, however, we have an initial reference state, the correlation

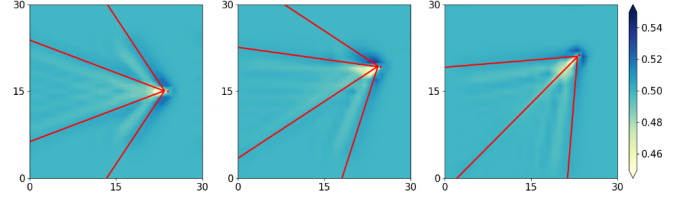


FIG. 5: Varying the angle of a moving potential compared to the lattice vectors. A potential moving at 0, 23, and 45 degrees with respect to the lattice. Here,  $\alpha = 1.7$ . A smeared potential (Gaussian with half a lattice spacing width) is used instead of a point potential to include effects when the tip is not precisely on a lattice site. Red lines represent the angles given by Eq. (29). Note that for motion at 45 degrees the angles for quadrants 1 and 4 in Eq. (29) coincide reducing the number of lines to 3.

matrix  $G_0$  of the unperturbed Fermi system, and in the following we consider the wake as a weak perturbation on this state, allowing us to analytically establish the dominant behavior of the wake pattern.

Since we are only perturbing the free evolution by a small potential, we can assume the steady state  $G$  will be close to the steady state of free evolution,  $G_0$ . Thus, we write  $G = G_0 + \delta G$  where  $\delta G$  is assumed a small perturbation. Since  $H_0$  is translation-invariant, we write the co-moving NESS equation in momentum space as:

$$e^{i\mathbf{a}\mathbf{w}\cdot(\mathbf{k}-\mathbf{k}')} \langle \mathbf{k} | e^{i\tau(H_0+V)} (G_0 + \delta G) e^{-i\tau(H_0+V)} | \mathbf{k}' \rangle = \langle \mathbf{k} | G_0 + \delta G | \mathbf{k}' \rangle$$

Substituting lowest order perturbation theory, keeping terms up to linear order in  $V$  and  $\delta G$ , we find that the real space density disturbance is given by:

$$\langle \mathbf{r} | \delta G | \mathbf{r} \rangle = \frac{V\tau\alpha^4}{(2\pi)^4} \int \int_{-\frac{\pi}{\alpha}}^{\frac{\pi}{\alpha}} d\mathbf{k} d\mathbf{k}' A(\mathbf{k}, \mathbf{k}') R(\mathbf{k}, \mathbf{k}', \mathbf{w}) \quad (10)$$

$$e^{i(\mathbf{r}_0 - \mathbf{r}) \cdot (\mathbf{k} - \mathbf{k}')} [\Theta(\varepsilon_f - \varepsilon(\mathbf{k})) - \Theta(\varepsilon_f - \varepsilon(\mathbf{k}'))]$$

where:

$$A(\mathbf{k}, \mathbf{k}') = \frac{e^{i\tau[\varepsilon(\mathbf{k}) - \varepsilon(\mathbf{k}')] - 1}}{\tau(\varepsilon(\mathbf{k}) - \varepsilon(\mathbf{k}'))}, \quad (11)$$

$$R(\mathbf{k}, \mathbf{k}', \mathbf{w}) = \frac{1}{1 - e^{-i\mathbf{a}\mathbf{w}\cdot(\mathbf{k}-\mathbf{k}')} e^{-i\tau[\varepsilon(\mathbf{k}) - \varepsilon(\mathbf{k}')]}} \quad (12)$$

and  $\varepsilon_f$  is the Fermi energy. Derivation details can be found in the supplementary material.

Our main objective now is to compute the large scale features of the resulting pattern, namely the typical angle that appears in the wake pattern. As in the case of the original Kelvin wake, which is typically derived by a stationary phase method, the present treatment requires careful consideration of the dominant contribution to the density variation [Eq. (10)]. The terms  $A$  and  $R$  in Eq. (10) will provide us with regions that are particularly important for the integral over  $\mathbf{k}$  and  $\mathbf{k}'$ . Due to

the Fermi functions, we can write Eq. (10) as:

$$\langle \mathbf{r} | \delta G | \mathbf{r} \rangle = \frac{2V\tau a^4}{(2\pi)^4} \int_{\varepsilon(\mathbf{k}) > \varepsilon_f} \int_{\varepsilon(\mathbf{k}') < \varepsilon_f} d\mathbf{k} d\mathbf{k}' \quad (13)$$

$$\text{Re} \left\{ A(\mathbf{k}, \mathbf{k}') R(\mathbf{k}, \mathbf{k}', \mathbf{w}) e^{i(\mathbf{r}_0 - \mathbf{r}) \cdot (\mathbf{k} - \mathbf{k}')} \right\}$$

Note that  $|A(\mathbf{k}, \mathbf{k}')| < 1$  (this follows from the inequality  $|e^{i\theta} - 1| \leq |\theta|$ ) and is dominated by  $\mathbf{k}, \mathbf{k}'$  near  $\varepsilon(\mathbf{k}) - \varepsilon(\mathbf{k}') = 0$ . We thus see that in contrast to the measurement and extraction wakes considered next, the integral is dominated by momenta near the Fermi surface since we can take such momenta to satisfy both conditions  $\tau(\varepsilon(\mathbf{k}) - \varepsilon(\mathbf{k}')) \ll 1$  and  $\varepsilon(\mathbf{k}) > \varepsilon_f$  and  $\varepsilon(\mathbf{k}') < \varepsilon_f$ .

We will henceforth consider the situation at half filling. Looking at the Fermi surface for our system, we break up the expansion around the Fermi surface into four quadrants given in Fig. 6. Close to the Fermi lines, we will use the variables  $\delta_y$  and  $\delta_{y'}$  instead of  $k_y, k'_y$  as the small shifts away from the Fermi surface. Explicitly,

Quadrant		
1	$k_y = \frac{\pi}{a} - k_x + \delta_y$	$k'_y = \frac{\pi}{a} - k'_x + \delta_{y'}$
2	$k_y = -\frac{\pi}{a} + k_x + \delta_y$	$k'_y = -\frac{\pi}{a} + k'_x + \delta_{y'}$
3	$k_y = \frac{\pi}{a} + k_x + \delta_y$	$k'_y = \frac{\pi}{a} + k'_x + \delta_{y'}$
4	$k_y = -\frac{\pi}{a} - k_x + \delta_y$	$k'_y = -\frac{\pi}{a} - k'_x + \delta_{y'}$

Let us now concentrate on  $R$  in Eq. (10). This term diverges when

$$\tau[\varepsilon(\mathbf{k}) - \varepsilon(\mathbf{k}')] + a\mathbf{w} \cdot (\mathbf{k} - \mathbf{k}') = 2\pi n \quad (15)$$

for  $n$  integer. Here we concentrate on the  $n = 0$  contribution which already recovers some basic features of the wake pattern, and leave the analysis of  $n \neq 0$  contributions for a future work. The equation can also be interpreted as a Mach-Cherenkov-Landau condition [23] for the momenta emitted by the wake due to creating a particle-hole excitation of momentum  $\mathbf{K} = \mathbf{k} - \mathbf{k}'$ . Perhaps a more familiar way to write the condition is:

$$\Omega(\mathbf{K}) + \mathbf{K} \cdot \mathbf{V} = 0 \quad (16)$$

where  $V = \tau^{-1}\alpha a\mathbf{w}$ , and  $\Omega(K) = \nabla_{\mathbf{k}}\epsilon(\mathbf{k})|_{k_F} \cdot \mathbf{K}$ .

For the square lattice, we have

$$\alpha a\mathbf{w} \cdot (\mathbf{k} - \mathbf{k}') = \cos(k_x a) + \cos(k_y a) - \cos(k'_x a) - \cos(k'_y a) \quad (17)$$

where  $\alpha$  is defined by Eq. 6. Now, combining the restriction  $\tau(\varepsilon(\mathbf{k}) - \varepsilon(\mathbf{k}')) \ll 1$  with Eq. (17), we find that

$$k'_x = k_x + w(k_y - k'_y) + \delta_x \quad (18)$$

where  $\delta_x$  is given by  $\delta_x \equiv \frac{\tau(\varepsilon(\mathbf{k}) - \varepsilon(\mathbf{k}'))}{a w_x}$  and where  $w \equiv \frac{w_y}{w_x}$ . Comparing to Eq. (14) we arrive at:

$$k_x = k'_x + \delta_{x'} \quad (19)$$

where  $\delta_{x'} \equiv \frac{w(\delta_y - \delta_{y'}) + \delta_x}{1 + (-1)^b w}$ . Here,  $b = 1$  for quadrant 1 and 4 (Fig. 6). Otherwise,  $b = 0$ . Note that our treatment of  $\delta_{x'}$  as small breaks down when  $w$  is close to 1. However, our final solution, Eq. (29), appears to still hold in this regime, and can be obtained by a different choice for the expansion parameters  $\delta_x, \delta_y$  above.

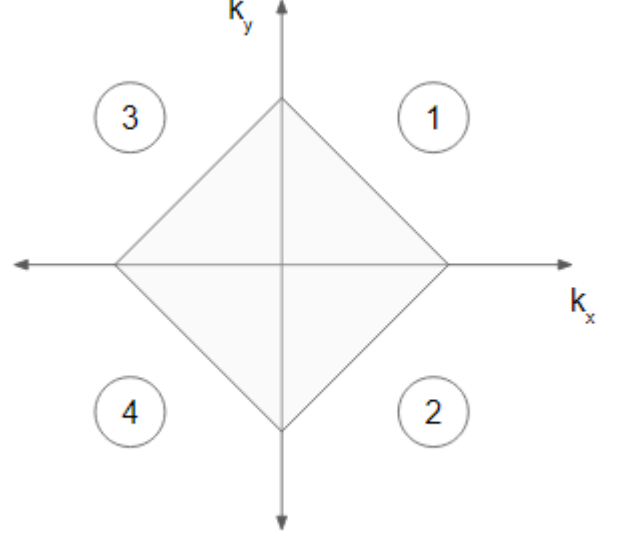


FIG. 6: Fermi surface at half-filling. At half filling all states with momenta  $k_x$  and  $k_y$  within the diamond shape are occupied. For the calculation we consider the four quadrants separately.

We now combine Eqs. (19), (14), and (17), and expand in small  $\delta_{x'}, \delta_y, \delta_{y'}$  to second order. Solving those, we can relate  $\delta_{x'}$  and  $\delta_{y'}$  to  $\delta_y$  and solve for  $k_x - k'_x$  and  $k_y - k'_y$  as

$$k_x - k'_x = \frac{2(w_x \alpha + \sin(ak_x))(w_y \alpha + (-1)^{b+1} \sin ak_x)}{(w_x + (-1)^b w_y) \alpha [(w_x + (-1)^{b+1} w_y) \alpha + 2 \sin(ak_x)]} \quad (20)$$

and

$$k_y - k'_y = \frac{2(w_x \alpha + \sin(ak_x))^2}{(w_x + (-1)^b w_y) \alpha [(w_x + (-1)^{b+1} w_y) \alpha + 2 \sin(ak_x)]} \quad (21)$$

If we assume our potential is at site  $\mathbf{r}_0 = (0,0)$ , the term  $e^{i(\mathbf{r}_0 - \mathbf{r}) \cdot (\mathbf{k} - \mathbf{k}')}$  in Eq. (13) becomes

$$e^{i(\mathbf{r}_0 - \mathbf{r}) \cdot (\mathbf{k} - \mathbf{k}')} \rightarrow e^{-i\mathbf{r} \cdot (\mathbf{k} - \mathbf{k}')} = e^{-i\delta_y B} \quad (22)$$

where

$$B = \frac{2[w_x \alpha + \sin(ak_x)]}{(w_x + (-1)^b w_y) \alpha [(w_x + (-1)^{b+1} w_y) \alpha + 2 \sin(ak_x)]} \times [r_x(w_y \alpha + (-1)^{b+1} \sin ak_x) + r_y(w_x \alpha + \sin ak_x)] \quad (23)$$

greatly reducing our momentum space integral to two coordinates,  $k_x$  and  $\delta_y$ . Note that when the denominators



in  $A, R$  in Eq. 13 vanish, the leading behavior of the combination  $AR$  is real, we arrive at:

$$\langle \mathbf{r} | \delta G | \mathbf{r} \rangle \propto -\frac{2V\tau a^4}{(2\pi)^4} \sum_{\mathcal{Q}} \text{Re} \left\{ \iint_{\mathcal{Q}} dk_x d\delta_y e^{i\delta_y B} \right\}, \quad (24)$$

where  $\mathcal{Q}$  is the set of four quadrants in Fig. 6. We have checked numerically that the integral (24) indeed captures the main wake pattern of the moving potential well. Our next task is to use Eq. (24) to find the main wake angles.

We now estimate analytically the main angles involved in the wake pattern left behind the moving potential. In the case of water wakes, we are interested in the wavefronts, which are lines of maximal disturbance. Here, we find that a more direct approach is to look instead for lines of zero disturbance, i.e.  $\langle \mathbf{r} | \delta G | \mathbf{r} \rangle = 0$ . We will begin by looking at the effects of individual quadrants in Eq. 24. Integrating over  $\delta_y$  and looking first at quadrant 1, we find

$$\begin{aligned} \langle \mathbf{r} | \delta G | \mathbf{r} \rangle &\propto -\frac{2V\tau a^2}{(2\pi)^4} \text{Re} \left\{ \int_0^{\pi/a} \int_0^{k_x} dk_x d\delta_y e^{i\delta_y B} \right\} \quad (25) \\ &= \frac{2V\tau a^2}{(2\pi)^4} \text{Im} \left\{ \int_0^{\pi/a} dk_x \frac{e^{ik_x B} - 1}{B} \right\} \end{aligned}$$

We now look for a situation where Eq. 25 tends to zero. Assuming that we could treat the equation by a stationary phase method, a condition for Eq. 25 vanishing would be that there exists a  $k_0$  such that  $k_x B \approx (k_x - k_0)^2$ . In this case, using the stationary phase approximation around  $k_0$  makes the dominant contribution to the integral in Eq. 25 real, and  $\langle \mathbf{r} | \delta G | \mathbf{r} \rangle$  vanishes. Specifically, for this to happen, we need  $B = 0$  and  $\frac{d}{dk_x} B = 0$  when evaluated at  $k_0$ . Looking at  $r_x, r_y \gg 1$ , i.e. far away from the potential, the dominating behavior of  $B$  comes from  $r_x(w_y\alpha + (-1)^{b+1} \sin ak_x) + r_y(w_x\alpha + \sin ak_x)$ . Hence, we find the equations:

$$r_x(w_y\alpha + (-1)^{b+1} \sin ak_x) + r_y(w_x\alpha + \sin ak_x) = 0, \quad (26)$$

and

$$(-1)^{b+1} r_x \cos ak_x + r_y \cos ak_x = 0. \quad (27)$$

Therefore,  $\cos ak_x = 0$  implying  $k_0 = \frac{\pi}{2a}$ . Plugging this into Eq. 26 yields

$$\frac{r_y}{r_x} = \frac{1 + w_y\alpha}{1 + w_x\alpha}. \quad (28)$$

Repeating this calculation for the other three quadrants, we find

Quadrant	Line of $\langle \mathbf{r}   \delta G   \mathbf{r} \rangle = 0$
1	$\frac{r_y}{r_x} = \frac{1 + w_y\alpha}{1 + w_x\alpha}$
2	$\frac{r_y}{r_x} = \frac{-1 + w_y\alpha}{1 + w_x\alpha}$
3	$\frac{r_y}{r_x} = \frac{1 + w_y\alpha}{-1 + w_x\alpha}$
4	$\frac{r_y}{r_x} = \frac{-1 + w_y\alpha}{-1 + w_x\alpha}$

(29)

and hence our main result Eq. (7). Figures 4 and 5 show agreement between the simulations of the potential wakes and our Eq. (29).

## MOVING PARTICLE EXTRACTOR AND MOVING DETECTORS

We proceed to consider a moving detector or particle extraction from the system. Note, that these processes are non-unitary. In this section we establish the co-moving steady-state for this problem. In particular, we show that in marked contrast with a moving potential, a moving detector at half filling does not generate a wake because of particle-hole symmetry.

We assume that the detection or extraction process is dominant when the tip is at a given site, but quickly weakens as the tip moves away from that site. It is therefore natural to discretize the process in such a way that we have a disturbance at a given site, followed by a free evolution of the system during a time  $\tau$  that the tip is traveling to the next site on its trajectory. The appropriate transformation rules  $\mathcal{K}(G)$  for detection and extraction are given in Eq. (3) and (4) respectively. If we allow for pure detection to happen with probability  $p$  (associated with the efficiency of the detector) and similarly extraction protocol with probability  $q$ , we can combine them, together with the free evolution  $U$  into the general form

$$G \rightarrow \mathcal{K}(G) = \mathcal{K}_U((1 - p - q)G + p\mathcal{K}_{\text{detect}}(G) + q\mathcal{K}_{\text{extract}}(G)) \quad (30)$$

which can be written as:

$$G \rightarrow \mathcal{K}(G) = U^\dagger [G - \gamma\{G, P\} + \xi PGP] U \quad (31)$$

where  $\xi = 2p + \epsilon^2 q$ ,  $\gamma = p + \epsilon q$ , and  $P$  is the projection onto a site  $\mathbf{r}_0$  where the tip acts. In particular, pure detection will be described by  $q = 0$ , hence  $\gamma = p$  and  $\xi = 2p$ .

In the next sections we work under the assumption that  $p, q \ll 1$  and hence  $\gamma \ll 1$ . The co-moving steady state equation (5) now reads:

$$\langle \mathbf{k} | S^\dagger U^\dagger [G - \gamma\{G, P\} + \xi PGP] U S | \mathbf{k}' \rangle = \langle \mathbf{k} | G | \mathbf{k}' \rangle$$

Written explicitly in momentum space we have:

$$e^{i\mathbf{a}\mathbf{w} \cdot (\mathbf{k} - \mathbf{k}')} e^{i\tau[\varepsilon(\mathbf{k}) - \varepsilon(\mathbf{k}')] } \{ \langle \mathbf{k} | G | \mathbf{k}' \rangle - \gamma \langle \mathbf{k} | \{G, P\} | \mathbf{k}' \rangle + \xi \langle \mathbf{k} | PGP | \mathbf{k}' \rangle \} = \langle \mathbf{k} | G | \mathbf{k}' \rangle$$

Assuming that  $\gamma \ll 1$ ,  $G \approx G_0 + \delta G$ , and zero temperature, we find that the local density variation is given by:

$$\begin{aligned} \langle \mathbf{r} | \delta G | \mathbf{r} \rangle &= \frac{\gamma a^4}{(2\pi)^4} \iint_{-\pi/a}^{\pi/a} d\mathbf{k} d\mathbf{k}' R(\mathbf{k}, \mathbf{k}', \mathbf{w}) e^{i(\mathbf{r}_0 - \mathbf{r}) \cdot (\mathbf{k} - \mathbf{k}')} \\ &\quad \left[ \frac{\xi \rho_f}{\gamma} - \Theta(\varepsilon_f - \varepsilon(\mathbf{k})) - \Theta(\varepsilon_f - \varepsilon(\mathbf{k}')) \right] \end{aligned} \quad (32)$$

where  $\rho_f$  is the density of fermions in  $G_0$  (i.e. the diagonal of the  $G_0$  matrix). Note, that like in the potential

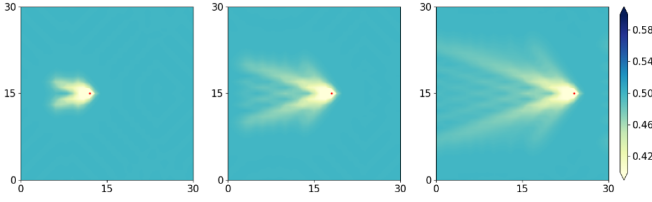


FIG. 7: A wake developing following a fermion extraction site moving at  $\alpha = 1.7$ . The pictures show a steady-state in the comoving frame.

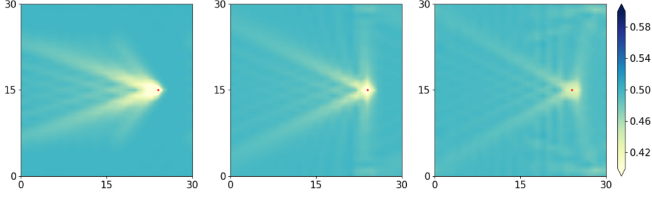


FIG. 8: Varying the speed of a moving particle extractor at half-filling. From left to right, speed  $\alpha = 1.7$ , 1.0, and 0.7 respectively.

case, the term  $R$  in Eq. (32) implies that Eq. (17) still characterizes a dominant region for the integral. However, Eq. (32) has two added difficulties when compared with the moving potential case Eq. (10). First, we no longer have the helpful constraint that  $\tau[\varepsilon(\mathbf{k}) - \varepsilon(\mathbf{k}')] \approx 0$ . Secondly,  $\varepsilon(\mathbf{k})$  and  $\varepsilon(\mathbf{k}')$  can now be on the same side of  $\varepsilon_f$  as well as on the opposite side. Nonetheless, the solution for a moving potential, Eq. (29), does appear to also describe the wake of a moving detector and extractor.

By iterating the evolution equation for the two point function  $G$ , the wake pattern can be generated numerically. For the case of a particle removal site moving through a half-filled Fermi sea we obtain the images shown in Fig. 7 and 8.

### Moving detector at half filling

Particle detection at half filling shows marked contrast with the density wake due to a moving potential. Indeed, due to particle hole symmetry it leaves the average density profile, namely the diagonal of  $G$  unchanged. On the other hand, a potential perturbation breaks particle-hole symmetry and generates the density wake described above.

In fact, we can establish a stronger property, namely:

$$\langle \mathbf{r} | \delta G | \mathbf{r} \rangle_\mu + \langle \mathbf{r} | \delta G | \mathbf{r} \rangle_{-\mu} = 0 \quad (33)$$

where  $\langle \mathbf{r} | \delta G | \mathbf{r} \rangle_\mu$  is obtained by successive applications of  $\mathcal{K}$  from Eq. (30) on an initial state  $G_0 = \frac{1}{1 + e^{\beta(H - \mu)}}$ , with  $q = 0$ , using an arbitrary choice of measuring site at each step, and in the end subtracting  $G_0$ . In other words,

changing the sign of the chemical potential changes the sign of the wake.

An immediate consequence of Eq. (33) is that at the point, where our many-body Hamiltonian has particle-hole symmetry, namely  $\mu = 0$  i.e. at half filling:

$$\langle \mathbf{r} | \delta G | \mathbf{r} \rangle_{\mu=0} = 0, \quad (34)$$

i.e. there should be no wake pattern created by a moving detector. This is shown in Fig. 9 by comparing a detector moving through a half-filled versus a quarter-filled Fermi sea. The image also shows how the quarter filled wake is opposite in sign to the wake generate in the Fermi system at three quarter filling.

A full non-perturbative proof of the remarkable relation (33) is presented in the supplementary material. Here for simplicity we establish (33) starting from the (zero temperature) perturbative result Eq. (32) with  $\epsilon_F = \mu$  and  $\xi = 2\gamma$ . Note that the sum  $\langle \mathbf{r} | \delta G | \mathbf{r} \rangle_\mu + \langle \mathbf{r} | \delta G | \mathbf{r} \rangle_{-\mu}$  is given by Eq. (32) with the term in brackets replaced with

$$2 - \Theta(\mu - \varepsilon(\mathbf{k})) - \Theta(\mu - \varepsilon(\mathbf{k}')) - \Theta(-\mu - \varepsilon(\mathbf{k})) - \Theta(-\mu - \varepsilon(\mathbf{k}')) \quad (35)$$

where we used that  $\rho_f(\epsilon_F) + \rho_f(-\epsilon_F) = 1$ .

Now consider the following map reflecting points about the Fermi surface:

$$\mathbf{k} \rightarrow \mathcal{M}(\mathbf{k}) \equiv (-1^b, -1^{1+Q}) \frac{\pi}{a} - \mathbf{k} \quad (36)$$

where  $Q$  is the quadrant number and  $b = 0$  if in quadrants 1 or 2 and  $b = 1$  in quadrants 3,4. Note that  $\epsilon(\mathcal{M}(\mathbf{k})) = -\epsilon(\mathbf{k})$ , and that,  $\exp[i\mathbf{r} \cdot (\mathcal{M}(\mathbf{k}) - \mathcal{M}(\mathbf{k}'))] = \exp[-i\mathbf{r} \cdot (\mathbf{k} - \mathbf{k}')] \exp[i\mathbf{r} \cdot (\mathcal{M}(\mathbf{k}) + \mathcal{M}(\mathbf{k}'))]$  thus, the real part of  $R(\mathbf{k}, \mathbf{k}', \mathbf{w}) e^{i(\mathbf{r}_0 - \mathbf{r}) \cdot (\mathbf{k} - \mathbf{k}')}$  in Eq. (32) is symmetric under such a transformation. On the other hand, the bracket term Eq. (35) is anti-symmetric under the map  $\mathcal{M}$ . The result of  $k, k'$  integrations will therefore vanish, establishing Eq. (33).

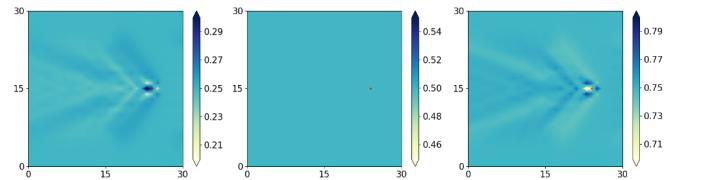


FIG. 9: Varying the density of fermions. From left to right, a detector moving at  $\alpha = 1.7$  for quarter-filling, half-filling, and three-quarter-filling, respectively. The color bar has the same scale but different offset.

### A "fluctuation" wake

The above results suggest at first glance that there is no effect of the detector at half filling. In fact, this is

not the case! While the moving detector does not affect the average density at half filling, it does perturb correlations, and thus may be observed through fluctuations. For example, such correlations may be observed by looking at the number of particles in a mode  $a_{A(\mathbf{r})}^\dagger \equiv \frac{1}{\sqrt{|A|}} \sum_{\mathbf{r}' \in A} a_{\mathbf{r}'}^\dagger$ , representing an equal weight superposition in a region lattice neighborhood  $A$  of a point  $\mathbf{r}$ . We have:

$$n_A(\mathbf{r}) \equiv \langle a_{A(\mathbf{r})}^\dagger a_{A(\mathbf{r})} \rangle = \frac{1}{|A|} \sum_{\mathbf{r}' \in A} G_{\mathbf{r}' \mathbf{r}'} = (37)$$

$$\frac{1}{|A|} \sum_{\mathbf{r}'' \in A} G_{0 \mathbf{r}''} + \frac{1}{|A|} \sum_{\mathbf{r}' \in A} \delta G_{\mathbf{r}' \mathbf{r}''}$$

We will focus on  $A$  being the set of nearest neighbors: an example of the wake in the density of the  $n_A(\mathbf{r})$  is then shown in Fig. 10. That this wake may be non-zero can be observed by generalizing Eq. (32) for off-diagonal elements. In this case, the only change to (32) is that  $e^{-i\mathbf{r} \cdot (\mathbf{k} - \mathbf{k}')} \rightarrow e^{-i(\mathbf{r} \cdot \mathbf{k} - \mathbf{r}' \cdot \mathbf{k}')}.$  Now, combining Eqs. (32) and Eq. (37), we find

$$e^{-i(\mathbf{r} \cdot \mathbf{k} - \mathbf{r}' \cdot \mathbf{k}')} \rightarrow e^{-i\mathbf{r} \cdot (\mathbf{k} - \mathbf{k}')} \sum_{q, q' \in \kappa} e^{-iq\mathbf{a} + iq'\mathbf{a}} \quad (38)$$

$$= e^{-i\mathbf{r} \cdot (\mathbf{k} - \mathbf{k}')} \left(1 - \frac{\varepsilon(\mathbf{k})}{t_{hop}}\right) \left(1 - \frac{\varepsilon(\mathbf{k}')}{t_{hop}}\right)$$

where  $\kappa = \{0, k_x, k_y, -k_x, -k_y\}$ .

Note, Eq. (38) is not symmetric under a reflection of  $\varepsilon(\mathbf{k}), \varepsilon(\mathbf{k}')$  about the Fermi energy. This implies that, unlike the diagonal of  $G_{rr}$ , the wake generated for the modes like  $A$  for a detector are non-zero.

A couple of remarks are in order.

(1) While we focused here on the density of the  $a_A^\dagger$  modes as an indicator of correlations, a more natural quantity for an experimental consideration is density-density correlations, and number fluctuations in the region  $A$ . A preliminary check shows that such number fluctuations will also exhibit a wake, which can be studied by considering the four-fermi correlation generalization of Eq. (2) and (3), which give a closed hierarchy of 4 point functions. This calculation will be presented in a future work. (2) A moving detector at half filling is an interesting example of a "hierarchy" of steady states. In this hierarchy, the local average density or "diagonal" of  $G$  at half filling is steady for any path a detector makes, and is thus in a steady state. However, the correlations depend on the trajectory of the detector and would, in general, not be in a steady state, moreover the many-body density matrix would not be in a steady state. It is not hard to construct examples where  $G$  is in a steady state, while the many body density matrix is time-dependent.

## FINITE TEMPERATURE STATES

In this section we analyze the effect of a non-zero temperature of the system on our moving disturbances. We assume that the system is prepared initially at finite temperature, and we neglect thermal dissipation on the time

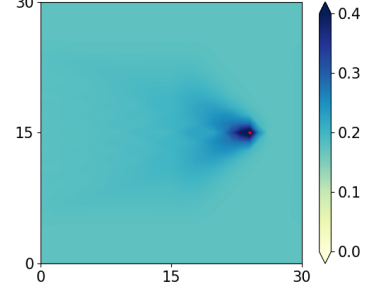


FIG. 10: Density of particles in a spatially spread mode following a moving detector at half-filling. Here we describe the density  $n_A(\mathbf{r})$  defined in Eq. (37).

scale of the motion of our disturbances. We find that at a generic filling the amplitude of the wakes are decreased, as may be expected on general grounds, i.e. with increased density fluctuations of the background. These results are shown in Figs. 11 and 12. Furthermore, we find that, at  $\rho_f = \frac{1}{2}$ , a moving detector continues to produce no wake at finite temperature. Perhaps the most surprising effect we find is that the extractor wake at half filling is temperature independent. This behavior is striking when compared to the moving potential source, see Fig. 11.

At finite temperature,  $\langle \mathbf{k} | G_0 | \mathbf{k}' \rangle = \delta_{\mathbf{k}\mathbf{k}'} F(\varepsilon(\mathbf{k}))$  instead of  $\delta_{\mathbf{k}\mathbf{k}'} \Theta(\varepsilon_f - \varepsilon(\mathbf{k}))$ , where  $F(\varepsilon(\mathbf{k}))$  is the Fermi-Dirac distribution. We find that the finite temperature steady states, are simply obtained by replacing the step functions in equations (10) and (32) by Fermi-Dirac functions  $F(\varepsilon(\mathbf{k}))$ .

Thus, the steady state of  $\delta G$  for a moving potential source, Eq. 10, becomes

$$\langle \mathbf{r} | \delta G | \mathbf{r} \rangle = \frac{V \tau a^4}{(2\pi)^4} \iint_{-\pi/a}^{\pi/a} d\mathbf{k} d\mathbf{k}' A(\mathbf{k}, \mathbf{k}') R(\mathbf{k}, \mathbf{k}', \mathbf{w}) e^{i(\mathbf{r}_0 - \mathbf{r}) \cdot (\mathbf{k} - \mathbf{k}')} [F(\varepsilon(\mathbf{k})) - F(\varepsilon(\mathbf{k}'))] \quad (39)$$

while for detection/extraction at finite temperature, Eq. 32 becomes

$$\langle \mathbf{r} | \delta G | \mathbf{r} \rangle = \frac{\gamma a^4}{(2\pi)^4} \iint_{-\pi/a}^{\pi/a} d\mathbf{k} d\mathbf{k}' R(\mathbf{k}, \mathbf{k}', \mathbf{w}) e^{i(\mathbf{r}_0 - \mathbf{r}) \cdot (\mathbf{k} - \mathbf{k}')} \left[ \frac{\xi \rho_f}{\gamma} - F(\varepsilon(\mathbf{k})) - F(\varepsilon(\mathbf{k}')) \right] \quad (40)$$

We can understand the temperature independence of the moving extractor at half filling as follows. Consider the difference between the moving extractor and moving detector steady state equations (Eq. (40) with  $\xi = 2\gamma$  and  $\xi = \gamma$  respectively), we find:

$$\langle \mathbf{r} | \delta G_{det} | \mathbf{r} \rangle - \langle \mathbf{r} | \delta G_{extr} | \mathbf{r} \rangle = \frac{\gamma a^4}{(2\pi)^4} \iint_{-\pi/a}^{\pi/a} d\mathbf{k} d\mathbf{k}' R(\mathbf{k}, \mathbf{k}', \mathbf{w}) e^{i(\mathbf{r}_0 - \mathbf{r}) \cdot (\mathbf{k} - \mathbf{k}')} \rho_f \quad (41)$$

Note, Eq. (41) depends only on the density  $\rho_f$ . Therefore the difference Eq. (41) is independent of temperature if



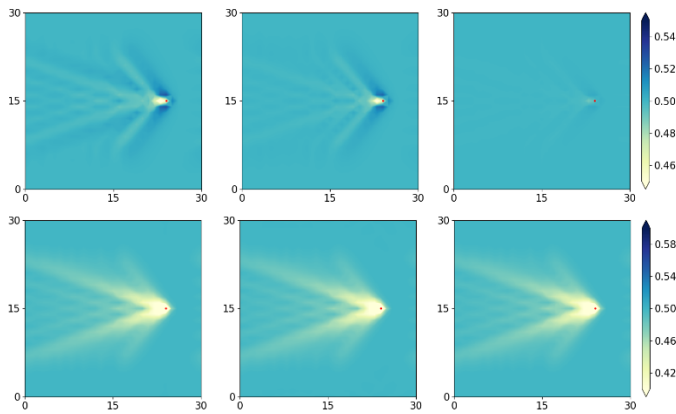


FIG. 11: Potential (top) and extraction (bottom) wakes at half-filling over varying temperature. From left to right,  $\frac{T}{t_{hop}} = 0, 1$ , and  $10$ .

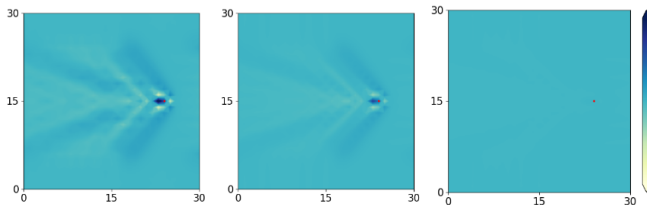


FIG. 12: Varying the temperature for detection wakes at quarter-filling. From left to right,  $\frac{T}{t_{hop}} = 0, 1$ , and  $10$ .

temperature is varied at a fixed density. Since detection creates no wake when  $\rho_f = \frac{1}{2}$  at any temperature, this implies that a moving particle extractor is temperature independent at  $\rho_f = \frac{1}{2}$ . This result matches simulations of the moving particle extractor as shown in Fig. 11.

## DISCUSSION OF EXPERIMENTAL REALIZATIONS

Here we consider a setup where the wakes may be explored in experiments with ultracold  $^6\text{Li}$  fermions in optical lattices. Quantum gas microscopes with single-particle and single-site resolution can directly observe the wake structure, as follows. The disturbance can be created by a focused laser beam with a waist on the order of the lattice spacing by employing a high-resolution objective [24]. We have checked by numerical simulations that using a Gaussian smeared potential instead of a point potential does not significantly alter wake geometry. Moreover, the wake pattern is not significantly changed if the initial Gaussian is not centered on a lattice site.

Because of the light mass of  $^6\text{Li}$  the timescales for Hubbard physics are still convenient for lattice spacing of approximately  $1\,\mu\text{m}$  [15] leading to moderate requirements of the objective ( $\text{NA} > 0.5$ ). A dynamically movable

disturbance can be implemented, for example, by piezo-actuated mirror mount or an acousto-optical deflector. An experimental run will then start with the preparation of a two-dimensional Fermi-Hubbard system and the movement of the focused laser beam through this system up to a certain position. Finally, the system is frozen by increasing the lattice depth and then imaged via fluorescence imaging. A single realization does not contain enough information to extract the details of the wake pattern. Reaching a density resolution of about 2% requires averaging about 2500 experimental realizations ( $1/\sqrt{n}$ ) while keeping track of the final position of the disturbance. The required precision and amount of data is comparable to recent experiments at existing quantum gas microscopes [15, 24]. The parameter  $\tau$  is proportional to the duration of beam motion, which should be compared to the hopping energy  $t_{hop}$ . It is possible to swipe the beam at different rates, to obtain various values of  $\alpha$  and the interesting regimes of  $\alpha < 1$  and  $\alpha > 1$  are accessible.

We note that all three types of disturbances can be implemented in experiments. A moving potential can be created by a far-detuned laser beam. A moving detector can be realized by a near-resonant laser beam. Scattering of photons at low intensity leads in good approximation to a measurement of the on-site particle density. Last, a particle extractor can be implemented via a defocused red-detuned optical dipole trap. Caused by the out-of-plane minimum in the potential, atoms will be sucked out-of-plane and will be lost in the experiment.

Beyond cold atoms, we expect the effects we predict to also hold in other systems which can be well describe by non-interacting fermions.

It is important to note that while the present discussion is focused on non-interacting systems, the formalism presented in [21] is valid also for systems prepared in an interacting state, as long as the subsequent step of unitary evolution while the tip is traveling between sites is well approximated by non-interacting evolution. Thus, a system prepared in a strongly correlated state, such as a Mott insulator, for example, that undergoes a quantum quench where interactions are turned off will still be described by the current method.

*Acknowledgments.* The work of I.K. and M.W. was supported in part by the NSF grant DMR-1508245.

- 
- [1] Amaresh Jaiswal and Victor Roy. Relativistic hydrodynamics in heavy-ion collisions: general aspects and recent developments. *Advances in High Energy Physics*, 2016, 2016.
  - [2] Haoyu Guo, Ekin Ilseven, Gregory Falkovich, and Leonid S Levitov. Higher-than-ballistic conduction of viscous electron flows. *Proceedings of the National Academy of Sciences*, 114(12):3068–3073, 2017.

- [3] JE Avron, B Gutkin, and DH Oaknin. Adiabatic swimming in an ideal quantum gas. *Physical review letters*, 96(13):130602, 2006.
- [4] Eugene B Kolomeisky and Joseph P Straley. Kelvin-mach wake in a two-dimensional fermi sea. *Physical review letters*, 120(22):226801, 2018.
- [5] Chiyan Luo, Mihai Ibanescu, Steven G Johnson, and JD Joannopoulos. Cerenkov radiation in photonic crystals. *science*, 299(5605):368–371, 2003.
- [6] Hongsheng Chen and Min Chen. Flipping photons backward: reversed cherenkov radiation. *Materials Today*, 14(1-2):34–41, 2011.
- [7] W. G. Unruh. Notes on black-hole evaporation. *Phys. Rev. D*, 14:870–892, Aug 1976.
- [8] Christian Gross and Immanuel Bloch. Quantum simulations with ultracold atoms in optical lattices. *Science*, 357(6355):995–1001, September 2017. Publisher: American Association for the Advancement of Science Section: Review.
- [9] Ariel Sommer, Mark Ku, Giacomo Roati, and Martin W. Zwierlein. Universal spin transport in a strongly interacting Fermi gas. *Nature*, 472(7342):201–204, apr 2011.
- [10] Marco Koschorreck, Daniel Pertot, Enrico Vogt, and Michael Köhl. Universal spin dynamics in two-dimensional fermi gases. *Nat. Phys.*, 9(7):405–409, may 2013.
- [11] S. Trotzky, S. Beattie, C. Luciuk, S. Smale, A.B. Bardson, T. Enss, E. Taylor, S. Zhang, and J.H. Thywissen. Observation of the Leggett-Rice effect in a unitary Fermi gas. *Phys. Rev. Lett.*, 114(1), jan 2015.
- [12] Sebastian Krinner, David Stadler, Dominik Huscsmann, Jean-Philippe Brantut, and Tilman Esslinger. Observation of quantized conductance in neutral matter. *Nature*, 517(7532):64–67, dec 2014.
- [13] Rhys Anderson, Fudong Wang, Peihang Xu, Vijin Venu, Stefan Trotzky, Frédéric Chevy, and Joseph H. Thywissen. Conductivity spectrum of ultracold atoms in an optical lattice. *Phys. Rev. Lett.*, 122:153602, Apr 2019.
- [14] W. Xu, W. R. McGehee, W. N. Morong, and B. DeMarco. Bad-metal relaxation dynamics in a Fermi lattice gas. *Nature Communications*, 10(1):1588, Apr 2019.
- [15] Jayadev Vijayan, Pimonpan Sompert, Guillaume Salomon, Joannis Koepsell, Sarah Hirthe, Annabelle Bohrdt, Fabian Grusdt, Immanuel Bloch, and Christian Gross. Time-resolved observation of spin-charge deconfinement in fermionic Hubbard chains. *Science*, 367(6474):186–189, January 2020. Publisher: American Association for the Advancement of Science Section: Report.
- [16] Matthew A. Nichols, Lawrence W. Cheuk, Melih Okan, Thomas R. Hartke, Enrique Mendez, T. Senthil, Ehsan Khatami, Hao Zhang, and Martin W. Zwierlein. Spin transport in a mott insulator of ultracold fermions. *Science*, 363(6425):383–387, 2019.
- [17] Peter T. Brown, Debayan Mitra, Elmer Guardado-Sanchez, Reza Nourafkan, Alexis Reymbaut, Charles-David Hébert, Simon Bergeron, A.-M. S. Tremblay, Jure Kokalj, David A. Huse, Peter Schauf, and Waseem S. Bakr. Bad metallic transport in a cold atom Fermi-Hubbard system. *Science*, 363(6425):379–382, 2019.
- [18] Lord Kelvin. On ship waves. *Proc. Inst. Mech. Engrs*, 38(1):409–434, 1887.
- [19] Alexandre Darmon, Michael Benzaquen, and Elie Raphaël. Kelvin wake pattern at large froude numbers. *Journal of Fluid Mechanics*, 738, 2014.
- [20] Jonathan Colen and Eugene B Kolomeisky. Kelvin-froude wake patterns of a traveling pressure disturbance. *arXiv preprint arXiv:1902.01884*, 2019.
- [21] Israel Klich. Closed hierarchies and non-equilibrium steady states of driven systems. *Annals of Physics*, 404:66–80, 2019.
- [22] Michael Bonitz. *Quantum kinetic theory*, volume 33. B. G. Teubner, Stuttgart- Leipzig, 1998.
- [23] Iacopo Carusotto and Germain Rousseaux. In Daniele Faccio et al., editors, *Analogue Gravity Phenomenology*, Lecture Notes in Physics, chapter 6, page 109. Springer International Publishing Switzerland, 2013. and references therein.
- [24] Christof Weitenberg, Manuel Endres, Jacob F. Sherson, Marc Cheneau, Peter Schauss, Takeshi Fukuhara, Immanuel Bloch, and Stefan Kuhr. Single-spin addressing in an atomic Mott insulator. *Nature*, 471(7338):319–324, March 2011.

### Derivation of the steady state Equations

Since we are only perturbing the free evolution by a small potential, we can assume the steady state  $G$  will be close to the steady state of free evolution,  $G_0$ . Thus, we write  $G = G_0 + \delta G$  where  $\delta G$  is assumed a small perturbation.

(1) **Moving potential.** In this case, our equation is:

$$e^{ia\mathbf{w} \cdot (\mathbf{k} - \mathbf{k}')} \langle \mathbf{k} | e^{i\tau(H_0+V)} (G_0 + \delta G) e^{-i\tau(H_0+V)} | \mathbf{k}' \rangle = \langle \mathbf{k} | G_0 + \delta G | \mathbf{k}' \rangle$$

Substituting lowest order perturbation theory,

$$e^{-i\tau(H_0+V)} \approx e^{-i\tau H_0} + ie^{-i\tau H_0} \int_0^\tau ds e^{isH_0} V e^{-isH_0} \quad (42)$$

and keeping terms up to linear order in  $V$  and  $\delta G$ , we find the equation

$$e^{ia\mathbf{w} \cdot (\mathbf{k} - \mathbf{k}')} \{ \langle \mathbf{k} | G_0 | \mathbf{k}' \rangle + \langle \mathbf{k} | e^{i\tau H_0} \delta G e^{-i\tau H_0} | \mathbf{k}' \rangle + \langle \mathbf{k} | e^{i\tau H_0} \left( i \int_0^\tau ds e^{isH_0} [G_0, V] e^{-isH_0} \right) e^{-i\tau H_0} | \mathbf{k}' \rangle \} \quad (43)$$

$$= \langle \mathbf{k} | G_0 | \mathbf{k}' \rangle + \langle \mathbf{k} | \delta G | \mathbf{k}' \rangle \quad (44)$$

Doing the  $s$  integral,

$$i \int_0^\tau ds e^{is[\varepsilon(\mathbf{k}) - \varepsilon(\mathbf{k}')] } = \frac{e^{i\tau[\varepsilon(\mathbf{k}) - \varepsilon(\mathbf{k}')] } - 1}{\varepsilon(\mathbf{k}) - \varepsilon(\mathbf{k}')}$$

and noting that  $(e^{ia\mathbf{w} \cdot (\mathbf{k} - \mathbf{k}')} - 1) \langle \mathbf{k} | G_0 | \mathbf{k}' \rangle = 0$  since  $G_0$  is diagonal in  $k$  we find

$$(e^{ia\mathbf{w} \cdot (\mathbf{k} - \mathbf{k}')} e^{i\tau[\varepsilon(\mathbf{k}) - \varepsilon(\mathbf{k}')] } - 1) \langle \mathbf{k} | \delta G | \mathbf{k}' \rangle = \frac{(e^{i\tau[\varepsilon(\mathbf{k}) - \varepsilon(\mathbf{k}')] } - 1) e^{ia\mathbf{w} \cdot (\mathbf{k} - \mathbf{k}')} e^{i\tau[\varepsilon(\mathbf{k}) - \varepsilon(\mathbf{k}')] }}{\varepsilon(\mathbf{k}) - \varepsilon(\mathbf{k}')} \langle \mathbf{k} | [G_0, V] | \mathbf{k}' \rangle \quad (45)$$

At zero temperature

$$\langle \mathbf{k} | G_0 V | \mathbf{k}' \rangle = G_0(\mathbf{k}) \langle \mathbf{k} | V | \mathbf{k}' \rangle = \Theta(\varepsilon_f - \varepsilon(\mathbf{k})) \sum_{\mathbf{r}} \langle \mathbf{k} | \mathbf{r} \rangle V(\mathbf{r}) \langle \mathbf{r} | \mathbf{k}' \rangle = \quad (46)$$

$$\frac{V}{vol} \Theta(\varepsilon_f - \varepsilon(\mathbf{k})) e^{i\mathbf{r}_0 \cdot (\mathbf{k} - \mathbf{k}')} , \quad (47)$$

where  $vol$  is the system volume. Thus,

$$\langle \mathbf{k} | \delta G | \mathbf{k}' \rangle = \frac{V (e^{i\tau[\varepsilon(\mathbf{k}) - \varepsilon(\mathbf{k}')] } - 1) e^{ia\mathbf{w} \cdot (\mathbf{k} - \mathbf{k}')} e^{i\tau[\varepsilon(\mathbf{k}) - \varepsilon(\mathbf{k}')] }}{vol[\varepsilon(\mathbf{k}) - \varepsilon(\mathbf{k}')] (e^{ia\mathbf{w} \cdot (\mathbf{k} - \mathbf{k}')} e^{i\tau[\varepsilon(\mathbf{k}) - \varepsilon(\mathbf{k}')] } - 1)} e^{i\mathbf{r}_0 \cdot (\mathbf{k} - \mathbf{k}')} [\Theta(\varepsilon_f - \varepsilon(\mathbf{k})) - \Theta(\varepsilon_f - \varepsilon(\mathbf{k}'))] \quad (48)$$

Finally, the real space number density variation is

$$\begin{aligned} \langle \mathbf{r} | \delta G | \mathbf{r} \rangle = & \\ \frac{V\tau a^4}{(2\pi)^4} \iint_{-\pi/a}^{\pi/a} d\mathbf{k} d\mathbf{k}' & \left[ \frac{e^{i\tau[\varepsilon(\mathbf{k}) - \varepsilon(\mathbf{k}')] } - 1}{\tau(\varepsilon(\mathbf{k}) - \varepsilon(\mathbf{k}'))} \right] \left[ \frac{1}{1 - e^{-ia\mathbf{w} \cdot (\mathbf{k} - \mathbf{k}')} e^{-i\tau[\varepsilon(\mathbf{k}) - \varepsilon(\mathbf{k}')] }} \right] e^{i(\mathbf{r}_0 - \mathbf{r}) \cdot (\mathbf{k} - \mathbf{k}')} [\Theta(\varepsilon_f - \varepsilon(\mathbf{k})) - \Theta(\varepsilon_f - \varepsilon(\mathbf{k}'))] \end{aligned} \quad (49)$$

(2) **Moving detection/extraction.** The co-moving steady state equation reads  $G = S^\dagger \mathcal{K}(\mathcal{G}) S$ . Written explicitly in momentum space we have:

$$e^{ia\mathbf{w} \cdot (\mathbf{k} - \mathbf{k}')} e^{i\tau[\varepsilon(\mathbf{k}) - \varepsilon(\mathbf{k}')] } \{ \langle \mathbf{k} | G | \mathbf{k}' \rangle - \gamma \langle \mathbf{k} | \{G, P\} | \mathbf{k}' \rangle + \xi \langle \mathbf{k} | PGP | \mathbf{k}' \rangle \} = \langle \mathbf{k} | G | \mathbf{k}' \rangle \quad (50)$$

Assuming that  $\gamma \ll 1$ ,  $G \approx G_0 + \delta G$ , and zero temperature,

$$\gamma \langle \mathbf{k} | GP | \mathbf{k}' \rangle \approx \gamma \langle \mathbf{k} | G_0 P | \mathbf{k}' \rangle = \frac{\gamma}{vol} \Theta(\varepsilon_f - \varepsilon(\mathbf{k})) e^{i\mathbf{r}_0 \cdot (\mathbf{k} - \mathbf{k}')} \quad (51)$$

Hence,

$$\gamma \langle \mathbf{k} | \{G, P\} | \mathbf{k}' \rangle \approx \frac{\gamma}{vol} e^{i\mathbf{r}_0 \cdot (\mathbf{k} - \mathbf{k}')} [\Theta(\varepsilon_f - \varepsilon(\mathbf{k})) + \Theta(\varepsilon_f - \varepsilon(\mathbf{k}'))] . \quad (52)$$

Now turning to the  $PGP$  term,

$$\langle \mathbf{k} | PG_0 P | \mathbf{k}' \rangle = \frac{a^2 vol}{(2\pi)^2} \int d\mathbf{q} \Theta(\varepsilon_f - \varepsilon(\mathbf{q})) \langle \mathbf{k} | P | \mathbf{q} \rangle \langle \mathbf{q} | P | \mathbf{k}' \rangle = \frac{a^2 vol}{(2\pi)^2} e^{i\mathbf{r}_0 \cdot (\mathbf{k} - \mathbf{k}')} \int d\mathbf{q} \Theta(\varepsilon_f - \varepsilon(\mathbf{q})) = \frac{\rho_f}{vol} e^{i\mathbf{r}_0 \cdot (\mathbf{k} - \mathbf{k}')} . \quad (53)$$

where  $\rho_f$  is the density of fermions for  $G_0$ .

Plugging Eqs. (52) and (53) into Eq. (50), we get

$$\langle \mathbf{k} | \delta G | \mathbf{k}' \rangle = \frac{\gamma}{vol} \left( \frac{e^{ia\mathbf{w} \cdot (\mathbf{k} - \mathbf{k}')} e^{i\tau[\varepsilon(\mathbf{k}) - \varepsilon(\mathbf{k}')]}}{e^{ia\mathbf{w} \cdot (\mathbf{k} - \mathbf{k}')} e^{i\tau[\varepsilon(\mathbf{k}) - \varepsilon(\mathbf{k}')]}} - 1 \right) \left[ \frac{\xi \rho_f}{\gamma} - \Theta(\varepsilon_f - \varepsilon(\mathbf{k})) - \Theta(\varepsilon_f - \varepsilon(\mathbf{k}')) \right] e^{i\mathbf{r}_0 \cdot (\mathbf{k} - \mathbf{k}')} . \quad (54)$$

Finally, the local density variation is given by:

$$\langle \mathbf{r} | \delta G | \mathbf{r} \rangle = \frac{\gamma a^4}{(2\pi)^4} \iint_{-\pi/a}^{\pi/a} d\mathbf{k} d\mathbf{k}' \left( \frac{1}{1 - e^{-ia\mathbf{w} \cdot (\mathbf{k} - \mathbf{k}')} e^{-i\tau[\varepsilon(\mathbf{k}) - \varepsilon(\mathbf{k}')]}} \right) e^{i(\mathbf{r}_0 - \mathbf{r}) \cdot (\mathbf{k} - \mathbf{k}')} \left[ \frac{\xi \rho_f}{\gamma} - \Theta(\varepsilon_f - \varepsilon(\mathbf{k})) - \Theta(\varepsilon_f - \varepsilon(\mathbf{k}')) \right] \quad (55)$$

which is Eq. (32) in the main text.

### Non-perturbative Results

In this section, we show that no detection wake is created at  $\rho_f = \frac{1}{2}$  and that the difference between detection and extraction is temperature independent even non-perturbatively.

We start by looking at a series of non-perturbative detections on  $G_0$ . A single detection at site  $\mathbf{r}$  and evolution for time  $\tau$  is

$$G = UP_r G_0 P_r U^\dagger + UP_r^\perp G_0 P_r^\perp U^\dagger \quad (56)$$

$$\equiv \sum_{a=\{0,1\}} P_r^a(\tau) G_0 P_r^a(\tau)$$

since  $[U, G_0] = 0$  and where  $P^0 \equiv P$ ,  $P^1 \equiv P^\perp$ , and  $UPU^\dagger \equiv P(\tau)$ .

Hence, after doing a series of  $m$  measurements, we have

$$G = \sum_{a_1, a_2, \dots, a_m} \left\{ \left[ \prod_{n=m, m-1, \dots, 1} P_{r_n}^{a_n}((m-n+1)\tau) \right] G_0 \left[ \prod_{n=1, 2, \dots, m} P_{r_n}^{a_n}((m-n+1)\tau) \right] \right\} \quad (57)$$

Looking at the diagonal of  $G$  in real space and inserting a resolution of identity,  $\int d\mathbf{q}_n |\mathbf{q}_n\rangle \langle \mathbf{q}_n|$ , to the right of every  $P_{r_n}^{a_n}$  sitting in the first term in brackets in Eq. (57) and inserting  $\int d\mathbf{q}'_n |\mathbf{q}'_n\rangle \langle \mathbf{q}'_n|$  to the left of every  $P_{r_n}^{a_n}$  sitting in the second bracketed term in Eq. (57) we find

$$\begin{aligned} \langle \mathbf{r} | G | \mathbf{r} \rangle \equiv \zeta_m(\mu) = & \int d\mathbf{k} d\mathbf{k}' e^{-i\mathbf{r} \cdot (\mathbf{k} - \mathbf{k}')} \int dQ dQ' \sum_{a_1, a_2, \dots, a_m} \left\{ \langle \mathbf{k} | P_{r_m}^{a_m}(\tau) | \mathbf{q}_m \rangle \langle \mathbf{q}_m | P_{r_{m-1}}^{a_{m-1}}(2\tau) | \mathbf{q}_{m-1} \rangle \dots \right. \\ & \times \langle \mathbf{q}_2 | P_{r_1}^{a_1}(m\tau) | \mathbf{q}_1 \rangle \langle \mathbf{q}_1 | G_0 | \mathbf{q}'_1 \rangle \langle \mathbf{q}'_1 | P_{r_1}^{a_1}(m\tau) | \mathbf{q}_2 \rangle \dots \langle \mathbf{q}'_m | P_{r_m}^{a_m}(\tau) | \mathbf{k}' \rangle \left. \right\} \end{aligned} \quad (58)$$

where  $\mu$  is the chemical potential. Now, focusing on only terms directly dependent on  $\mathbf{q}_1, \mathbf{q}'_1$  and denoting all other terms by  $B$ , we find

$$\begin{aligned}
\zeta_m(\mu) &= B \int d\mathbf{q}_1 d\mathbf{q}'_1 \sum_{a_1} \langle \mathbf{q}_2 | P_{r_1}^{a_1}(m\tau) | \mathbf{q}_1 \rangle \langle \mathbf{q}_1 | G_0 | \mathbf{q}'_1 \rangle \langle \mathbf{q}'_1 | P_{r_1}^{a_1}(m\tau) | \mathbf{q}'_2 \rangle \\
&= B \int d\mathbf{q}_1 \sum_{a_1} \langle \mathbf{q}_2 | P_{r_1}^{a_1}(m\tau) | \mathbf{q}_1 \rangle F_\mu(\varepsilon(\mathbf{q}_1)) \langle \mathbf{q}_1 | P_{r_1}^{a_1}(m\tau) | \mathbf{q}'_2 \rangle \\
&= B \int d\mathbf{q}_1 e^{im\tau[\varepsilon(\mathbf{q}_2) - \varepsilon(\mathbf{q}'_2)]} F_\mu(\varepsilon(\mathbf{q}_1)) \left[ \delta_{\mathbf{q}_1 \mathbf{q}_2} \delta_{\mathbf{q}_1 \mathbf{q}'_2} + e^{i\mathbf{r}_1 \cdot (\mathbf{q}_2 - \mathbf{q}'_2)} (2 - \delta_{\mathbf{q}_1 \mathbf{q}_2} - \delta_{\mathbf{q}_1 \mathbf{q}'_2}) \right] \\
&= \zeta_{m-1}(\mu) + B \int d\mathbf{q}_1 e^{im\tau[\varepsilon(\mathbf{q}_2) - \varepsilon(\mathbf{q}'_2)]} F_\mu(\varepsilon(\mathbf{q}_1)) e^{i\mathbf{r}_1 \cdot (\mathbf{q}_2 - \mathbf{q}'_2)} (2 - \delta_{\mathbf{q}_1 \mathbf{q}_2} - \delta_{\mathbf{q}_1 \mathbf{q}'_2}) \\
&= \zeta_{m-1}(\mu) + B e^{im\tau[\varepsilon(\mathbf{q}_2) - \varepsilon(\mathbf{q}'_2)]} e^{i\mathbf{r}_1 \cdot (\mathbf{q}_2 - \mathbf{q}'_2)} (2\rho_f - F_\mu(\varepsilon(\mathbf{q}_2)) - F_\mu(\varepsilon(\mathbf{q}'_2)))
\end{aligned} \tag{59}$$

Now, we look at  $\zeta_m(\mu) + \zeta_m(-\mu)$  in a way analogous to Eq. (35) in the main text. Here, we find

$$\begin{aligned}
&\zeta_m(\mu) + \zeta_m(-\mu) = \zeta_{m-1}(\mu) + \zeta_{m-1}(-\mu) \\
&+ B \left\{ e^{im\tau[\varepsilon(\mathbf{q}_2) - \varepsilon(\mathbf{q}'_2)]} e^{i\mathbf{r}_1 \cdot (\mathbf{q}_2 - \mathbf{q}'_2)} (2 - F_\mu(\varepsilon(\mathbf{q}_2)) - F_\mu(\varepsilon(\mathbf{q}'_2))) - F_{-\mu}(\varepsilon(\mathbf{q}_2)) - F_{-\mu}(\varepsilon(\mathbf{q}'_2))) \right\}
\end{aligned} \tag{60}$$

Note, the real part of the term in braces in Eq. (60) is anti-symmetric under the transformation  $\mathbf{q} \rightarrow \mathcal{M}(\mathbf{q})$ , where  $\mathbf{q}$  here represents all  $\mathbf{q}_n$ ,  $\mathbf{q}'_n$ ,  $\mathbf{k}$ , and  $\mathbf{k}'$ . Let us now look at the term  $B$ . Note, explicitly,

$$B = \int dQ_1 dQ'_1 e^{-i\mathbf{r} \cdot (\mathbf{q}_{m+1} - \mathbf{q}'_{m+1})} \sum_{a_2, \dots, a_m} \prod_{n=m+1, m, \dots, 2} \langle \mathbf{q}_n | P_{r_{n-1}}^{a_{n-1}}((m-n+2)\tau) | \mathbf{q}_{n-1} \rangle \langle \mathbf{q}'_{n-1} | P_{r_{n-1}}^{a_n}((m-n+2)\tau) | \mathbf{q}'_n \rangle \tag{61}$$

where  $dQ_1$  and  $dQ'_1$  are defined by  $\prod_{n=2, \dots, m+1} d\mathbf{q}_n$  and  $\prod_{n=2, \dots, m+1} d\mathbf{q}'_n$  respectively. Also, here we define  $\mathbf{q}_{m+1} \equiv \mathbf{k}$  and  $\mathbf{q}'_{m+1} \equiv \mathbf{k}'$ .

Simplifying  $B$ , we find

$$\begin{aligned}
B &= \int dQ_1 dQ'_1 e^{-i\mathbf{r} \cdot (\mathbf{q}_{m+1} - \mathbf{q}'_{m+1})} \prod_{n=m+1, m, \dots, 2} e^{i(m-n+2)\tau[\varepsilon(\mathbf{q}_n) - \varepsilon(\mathbf{q}_{n-1}) + \varepsilon(\mathbf{q}'_{n-1}) - \varepsilon(\mathbf{q}'_n)]} \\
&\times \left[ \delta_{\mathbf{q}_n \mathbf{q}_{n-1}} \delta_{\mathbf{q}'_n \mathbf{q}'_{n-1}} - e^{i\mathbf{r}_{n-1} \cdot (\mathbf{q}_n - \mathbf{q}_{n-1})} \delta_{\mathbf{q}'_n \mathbf{q}'_{n-1}} - e^{i\mathbf{r}_{n-1} \cdot (\mathbf{q}'_{n-1} - \mathbf{q}'_n)} \delta_{\mathbf{q}_n \mathbf{q}_{n-1}} + 2e^{i\mathbf{r}_{n-1} \cdot (\mathbf{q}_n - \mathbf{q}_{n-1})} e^{i\mathbf{r}_{n-1} \cdot (\mathbf{q}'_{n-1} - \mathbf{q}'_n)} \right]
\end{aligned} \tag{62}$$

It can now be seen from Eq. (62) that  $B$  is symmetric under the transformation  $\mathbf{q} \rightarrow \mathcal{M}(\mathbf{q})$ . Since  $B$  is symmetric and the term in braces in Eq. (60) is anti-symmetric, we find

$$\zeta_m(\mu) + \zeta_m(-\mu) = \zeta_{m-1}(\mu) + \zeta_{m-1}(-\mu) \tag{63}$$

Thus,  $\zeta_m(\mu) + \zeta_m(-\mu) = \zeta_0(\mu) + \zeta_0(-\mu) = 1$  and

$$\langle \mathbf{r} | G | \mathbf{r} \rangle_\mu = 1 - \langle \mathbf{r} | G | \mathbf{r} \rangle_{-\mu} \tag{64}$$

i.e. the detection wake for a chemical potential of  $\mu$  is one minus the detection wake for a chemical potential of  $-\mu$ . Hence, when  $\mu = 0$  there is no detection wake. We emphasize that this result assumed no particular path for the moving detector.

Turning to a moving extractor, note that for the difference between the extractor and detector wake, we get Eq. (57) where we set  $a_1, a_2, \dots, a_m = 0$ . Thus, Eq. (60) becomes

$$\zeta_m = B \int d\mathbf{q}_1 e^{im\tau[\varepsilon(\mathbf{q}_2) - \varepsilon(\mathbf{q}'_2)]} \delta_{\mathbf{q}_1 \mathbf{q}'_1} F(\varepsilon(\mathbf{q}_1)) e^{i\mathbf{r}_1 \cdot (\mathbf{q}_2 - \mathbf{q}'_2)} = B e^{im\tau[\varepsilon(\mathbf{q}_2) - \varepsilon(\mathbf{q}'_2)]} e^{i\mathbf{r}_1 \cdot (\mathbf{q}_2 - \mathbf{q}'_2)} \rho_f \tag{65}$$

Hence, the difference between a moving detector and moving extractor is temperature independent non-perturbatively. Similar to the perturbative case, this implies that a moving particle extractor at  $\rho_f = \frac{1}{2}$  is temperature independent. Again, note that we have assumed no particular path for our moving particle extractor.



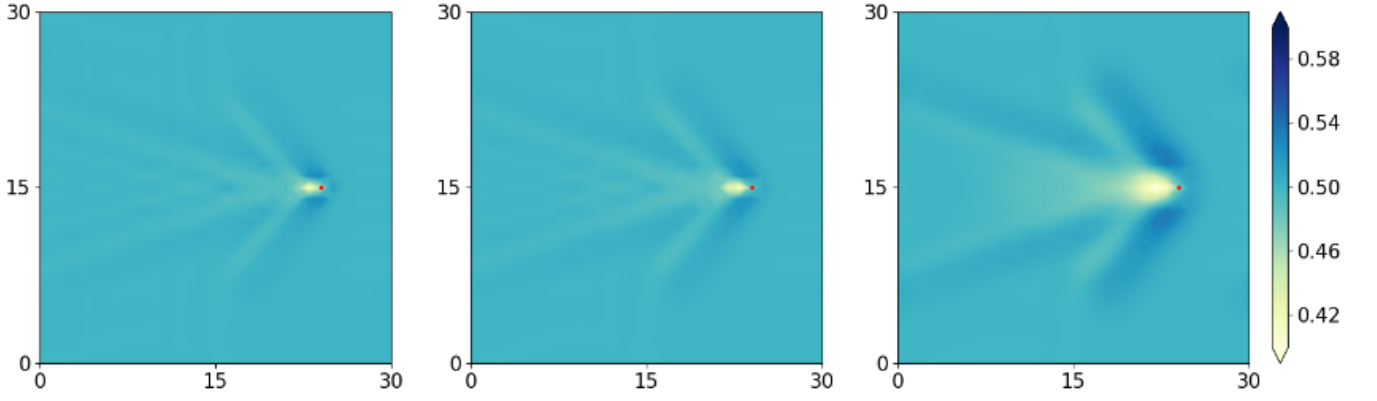


FIG. 13: A gaussian potential at half-filling and  $\alpha = 1.7$ . From left to right, the standard deviation of the gaussian in terms of lattice spacing,  $a$ , is point potential,  $0.5a$ , and  $a$ .

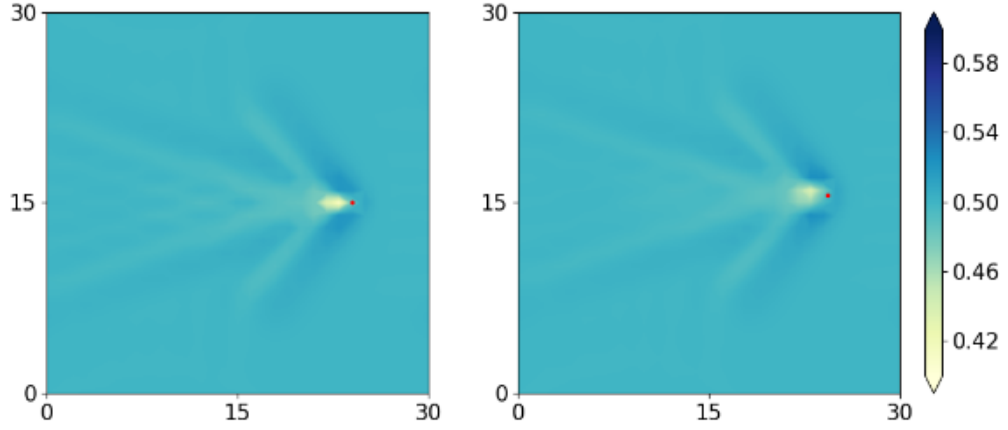


FIG. 14: A gaussian potential at half-filling,  $\alpha = 1.7$ , and  $0.5a$  standard of deviation where  $a$  is the lattice spacing. Left is a gaussian starting directly on lattice site (8,15). Right is a gaussian starting in-between lattice sites at (8.3,15.6).

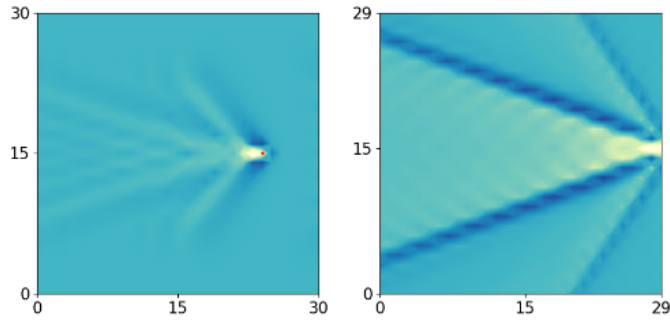


FIG. 15: Comparison of potential wake at half-filling for  $\alpha = 1.7$  for simulation (left) and numerical integration of Eq. (24) (right).